Electronic Supplementary Material (ESI) for Journal of Materials Chemistry C.

Elementary Supporting Information

Enhancement of charge-generation efficiency for naphthalene diimide-based polymer semiconductor by using pyrene-substituted *n*-dopant

Minghao Liang,† Yan Zeng,† Wansong Shang, Yuanping Yi, Cheng Li, Xi-Sha Zhang, Guanxin Zhang,* Deqing Zhang*

1. Materials and characterization techniques

All chemical reagents without any notes were commercially available and used as

received. N-DMBI and N2200 was purchased from One-Material.

^{1}H and ^{13}C NMR spectra were recorded on Bruker Advance (400 MHz) spectrometers. UV-Vis-NIR absorption spectra were acquired using a spectrophotometer (HITACHI UH4150). Atomic Force Microscope (AFM) images were recorded using a Digital Instruments Nano scope IIIa multimode atomic force microscope in taping mode under ambient conditions. Two-dimensional grazing incidence wide angle X-ray scattering (GIWAXS) measurements were conducted on a Xenocs SAXS/WAXS system with X-ray wavelength of 1.5418 Å and the films samples were irradiated at a fixed angle of 0.2°. The electron paramagnetic resonance (EPR) measurements were performed on a Bruker-EMX EPR spectrometer at room temperature. Spin counting was conducted by comparing with standard samples (tempo) with known numbers of spins following standard procedures.[s1] The film thickness was determined using Bruker Dektak XT. IR spectra were recorded on a JASCO FT/IR-480 plus Fourier transform infrared spectrometer.

2. Synthesis of Py-DMBI

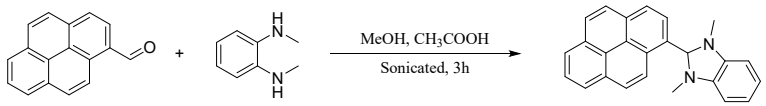

Py-DMBI

Scheme S1. Synthetic route for Py-DMBI

Synthesis of Py-DMBI: Under a nitrogen atmosphere, pyrenecarboxaldehyde (0.46 g, 2.0 mmol) and *N, N*-dimethylbenzene-1,2-diamine (0.27 g, 2.0 mmol) was added to the methanol solution (4 mL) containing two drops of acetic acid under N_2. Then the mixture was sonicated for 3h. After reaction, the mixture was filtered and washed with methanol, and dried in vacuum at 60 ^{o}C for 12 h. At last, faint yellow solid was obtained in 85% yield. ^{1}H NMR (400 MHz, DMSO-*d6*): δ 8.89 (d, J = 9.2 Hz, 1H), 8.41-8.33 (m, 4H), 8.31-8.26 (m, 2H), 8.21 (d, J = 9.4 Hz, 1H), 8.14 (t, J = 7.6 Hz, 1H), 6.76-6.74 (m, 2H), 6.61-6.59 (m, 2H), 5.95 (s, 1H), 2.56 (s, 6H). ^{13}C NMR (100 MHz, DMSO-*d6*): δ 142.51, 132.06, 131.83, 131.22, 130.59, 128.39, 127.87, 126.86, 126.00, 125.93, 125.23, 124.38, 119.72, 106.48, 33.85, 33.81. Elemental analysis: calcd. for $C_{25}H_{20}N_2$: C, 86.17; H, 5.79; N, 8.04; Found: C, 85.81; H, 5.83; N, 7.99.

3. The frontier molecular orbitals of tetramer of PNDI2TEG-2Tz and corresponding energy level

In order to figure out the origin of absorption spectra of **PNDI2TEG-2Tz,** the tetramer of **PNDI2TEG-2Tz** was selected and studied. The conformation of tetramer of **PNDI2TEG-2Tz** was selected and optimized at the B3LYP-D3(BJ)/6-31G** level. Then, the vertical electronic excitation energies were calculated using time-dependent density functional theory (TDDFT), and 30 lowest-lying singlet excited states were considered at the same level of theory. To simplify the calculation, long alkyl chains and ethylene glycol chain were replaced with methyl groups and -CH_2OCH_3, respectively.

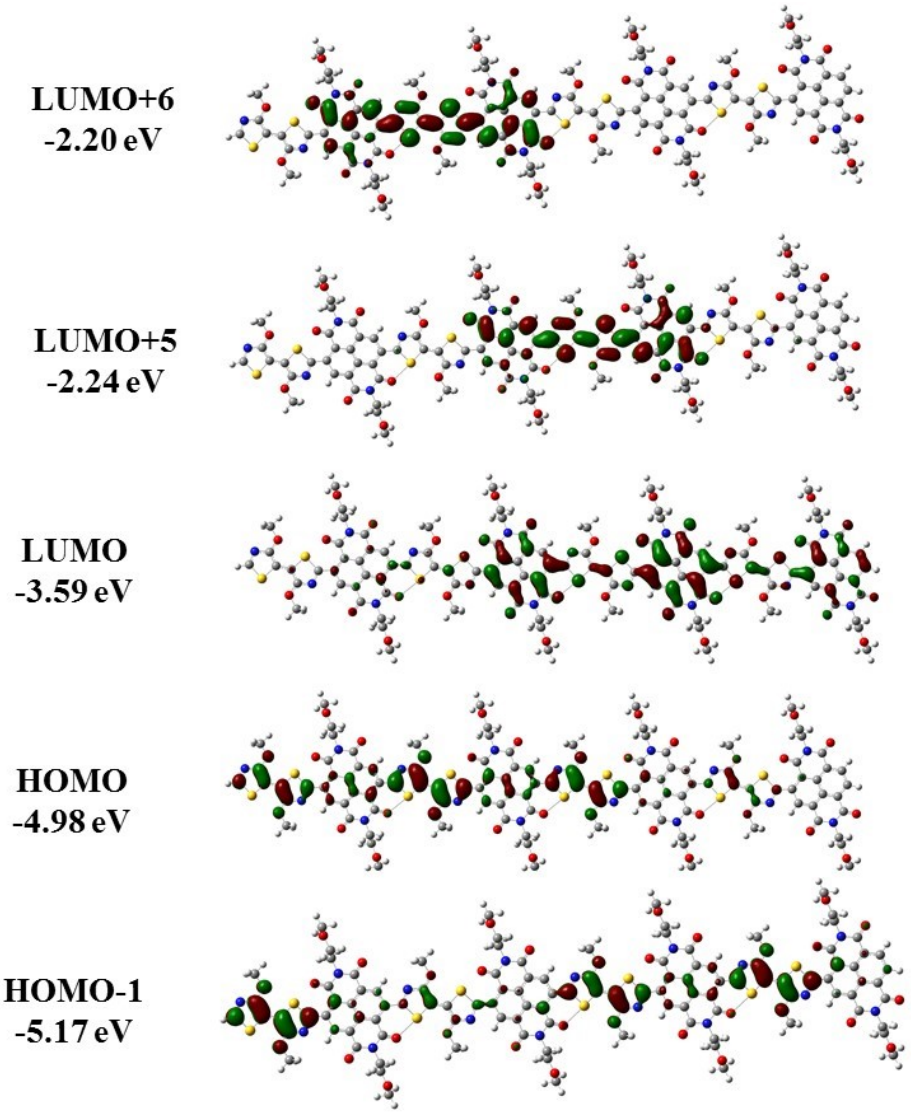

Fig. S1 The frontier molecular orbitals of **PNDI2TEG-2Tz** tetramer and corresponding energy levels.

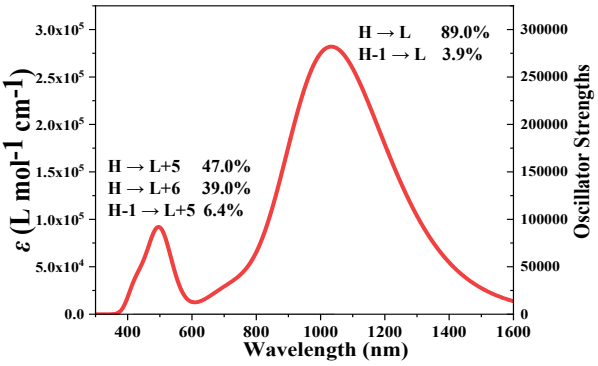

Fig. S2 The calculated absorption spectra of PNDI2TEG-2Tz tetramer.

4. Variation of absorption spectra of chloroform solution and thin films of PNDI2TEG-2Tz containing N-DMBI and Py-DMBI, respectively

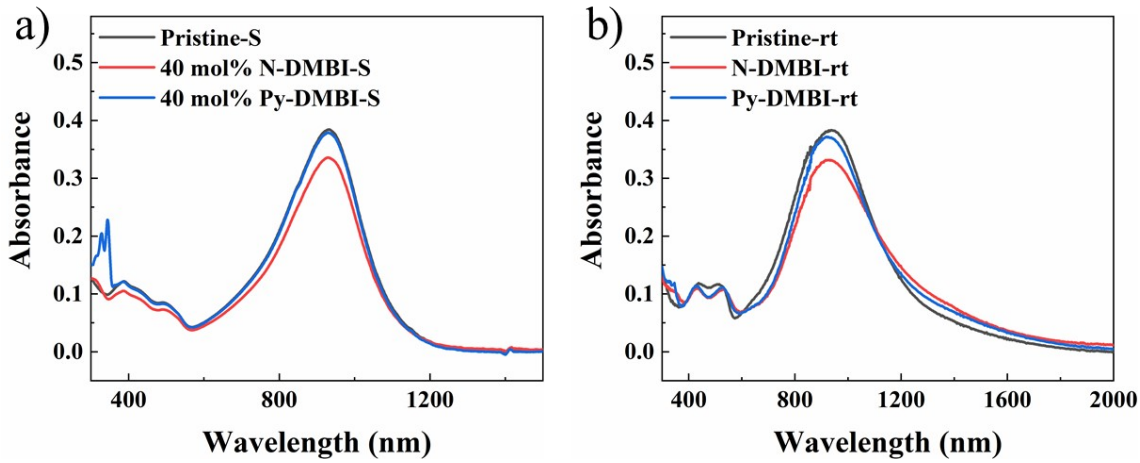

Fig. S3 a, b) Absorption spectra of $CHCl_3$ solution (a) and film (b) of PNDI2TEG-2Tz containing 40 mol% N-DMBI and Py-DMBI at room temperature, respectively. 'S' refers to solution; while 'rt' refers to room temperature which means the films those prepared and measured at room temperature.

4. Characterization of thermoelectric performances

PNDI2TEG-2Tz or N2200 was dissolved in $CHCl_3$ at a concentration of 10 mg/mL and 5 mg/mL, respectively, and then blended with a dopant solution at room temperature, varying the doping ratio. Devices for measuring conductivity and Seebeck coefficient were fabricated on glass substrates. Thin films were deposited on the treated substrates by spin-coating the mixed solution at 2000 rpm for 60 seconds and annealed at 140°C for 2 hours. The in-plane conductivity was measured using four-probe measurements in a N_2 glove box with a Keithley 4200 SCS semiconductor parameter analyzer. The film thickness was

determined using Bruker Dektak XT. Four-point measurements were conducted to determine the electrical resistivity with Agilent B1500A. The temperature gradient was introduced by Peltier Element. An infrared camera (temperature sensitivity＜50 mK) was used to measure the temperature difference between two electrode. Seebeck coefficient can be calculated by S=ΔV/ΔT, where ΔV is the thermal voltage between the two electrodes of the device when applied a temperature of ΔT. The ΔV is measured by Agilent B1500 under vacuum. The device architecture for measuring conductivity and Seebeck coefficients is shown below.

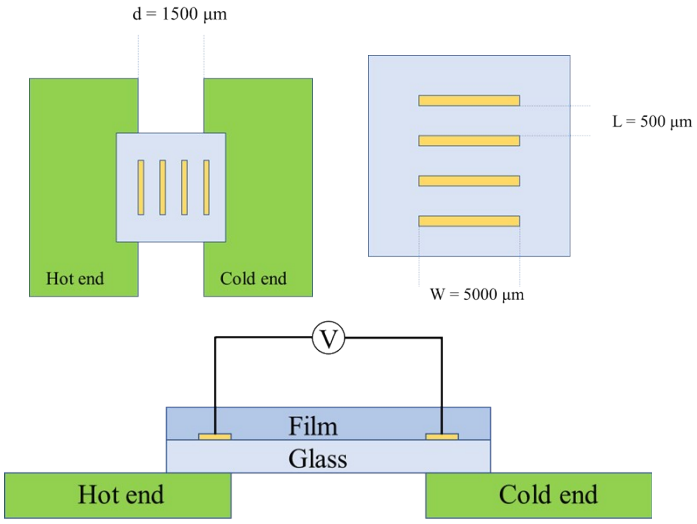

Fig.S4 The device architecture for measuring conductivity and Seebeck coefficients.

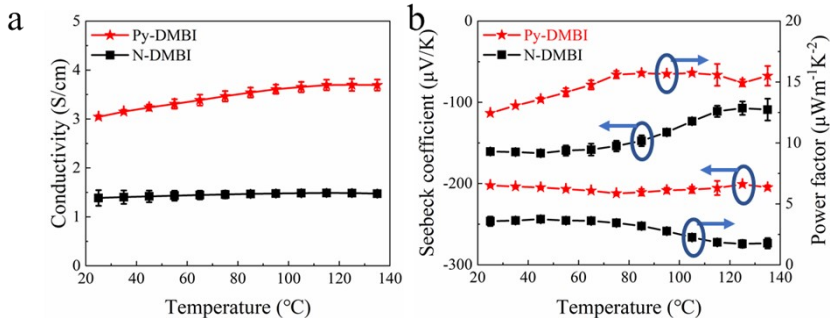

Fig. S5 a) The electrical conductivities and b) Seebeck coefficient and power factor of PNDI2TEG-2Tz doped by N-DMBI at 30 mol% (*vs.* the repeat unit of PNDI2TEG-2Tz) and Py-DMBI 20 mol% (*vs.* the repeat unit of PNDI2TEG-2Tz) at different temperatures. All the films were thermally annealed at 140 °C for 2 hours before the measurements.

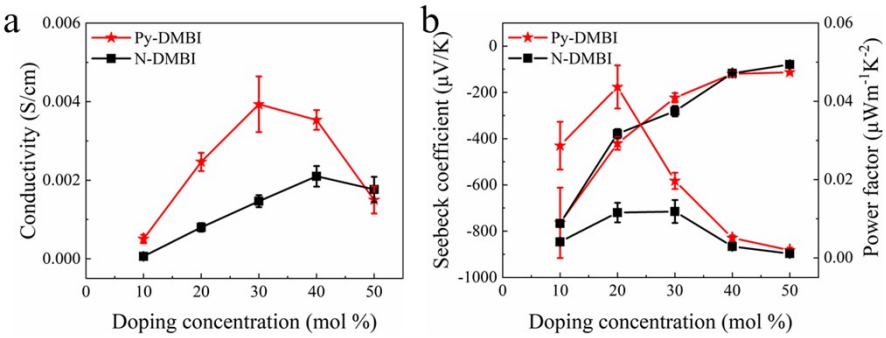

Fig. S6 a) The electrical conductivities and b) Seebeck coefficient and power factor of pristine and N2200 doped by N-DMBI and Py-DMBI at different molar ratios vs the repeat unit of PNDI2TEG-2Tz. All the films were thermally annealed at 140 °C for 2 hours before the measurements.

5. GIWAXS patterns

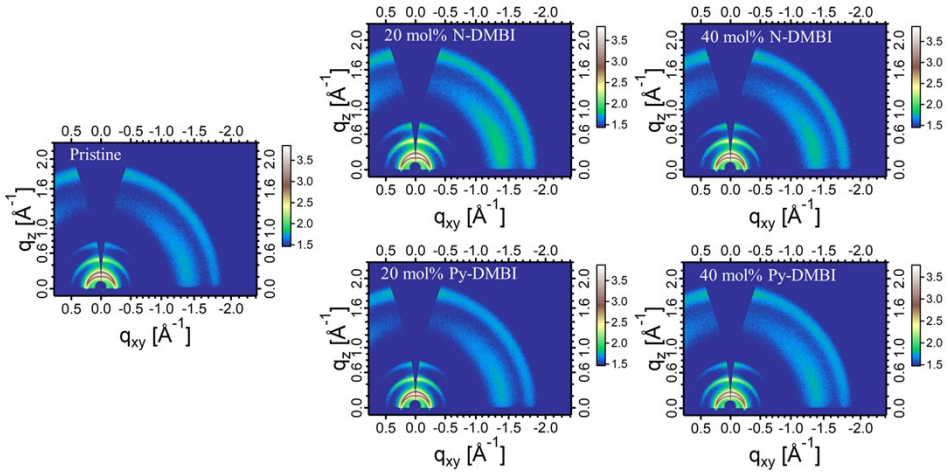

Fig. S7 GIWAXS patterns of PNDI2TEG-2Tz doped with N-DMBI and Py-DMBI at different molar ratios (*vs.* the repeat unit of PNDI2TEG-2Tz), respectively. All the films were thermally annealed at 140 °C for 2 hours before the measurements.

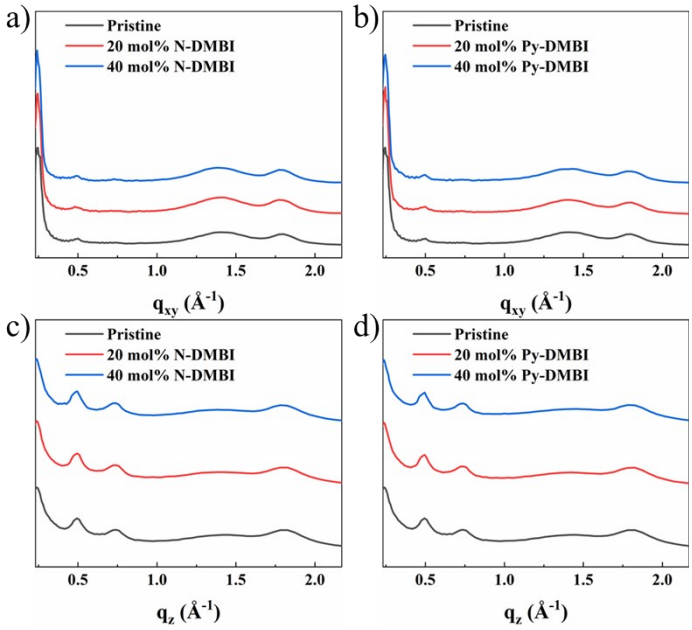

Fig. S8 The *in-plane* (a, b) and *out-of-plane* (c, d) profiles of the corresponding GIWAXS patterns of PNDI2TEG-2Tz doped with N-DMBI and Py-DMBI at different molar ratios (*vs.* the repeat unit of PNDI2TEG-2Tz).

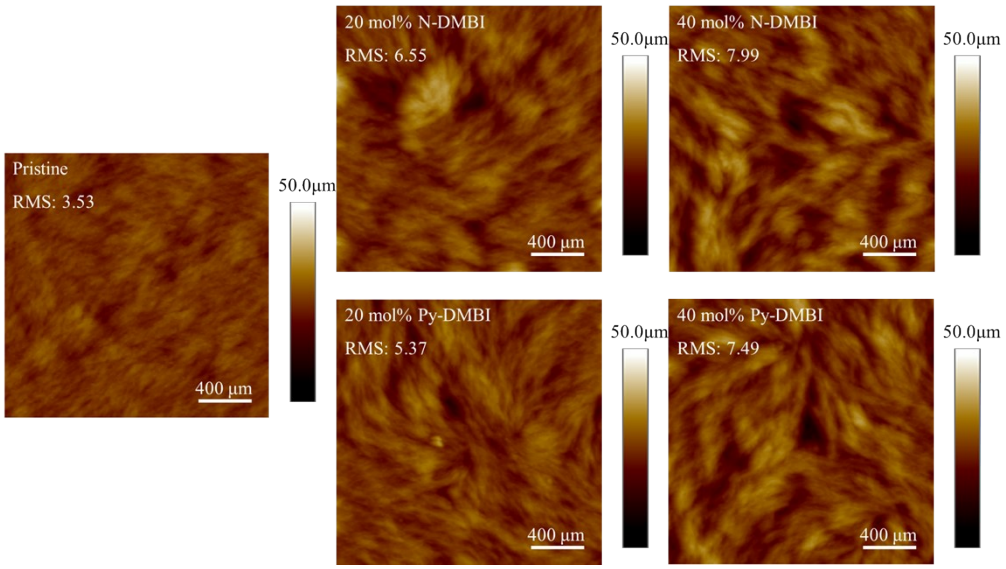

Fig. S9 AFM height images of PNDI2T2G-2Tz thin films before and after doped with the dopants at 20 mol% and 40 mol% (*vs.* the repeat unit of PNDI2TEG-2Tz), respectively.

6. Scanning near-field optical microscopy (SNOM) images of pristine film of PNDI2T2G-2Tz, film of PNDI2T2G-2Tz containing 40 mol% PyDMBI and that containing 40 mol% N-DMBI before annealing, respectively

We used scanning near-field optical microscopy (s-SNOM) to study the distribution of dopants in the film of PNDI2TEG-2Tz. The infrared near-field microscopy was setted up based on a commerical s-SNOM (neaSNOM from neaspec GmbH), which employs a tuneable MirCat quantum cascade laser (QCL) for s-SNOM imaging. The laser beams are focussed onto a standard platinum-coated AFM tip (NCPt arrow tip, Nanoworld), which is in close proximity to the sample. The AFM tip acts as an optical antenna and creates strongly enhanced near fields around the tip apex, yielding a spatial resolution (10 nm-20 nm) in the order of the tip radius.

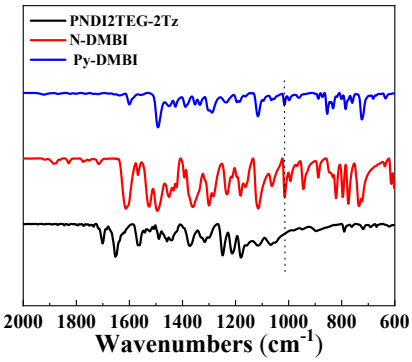

Fig. S10 Infrared spectra of PNDI2T2G-2Tz, N-DMBI and Py-DMBI, respectively.

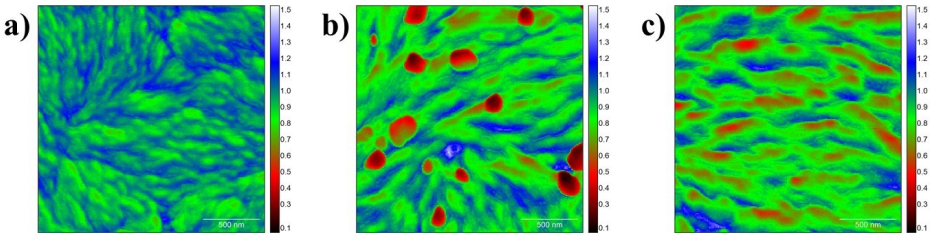

Fig.S11 SNOM images of pristine film of PNDI2T2G-2Tz (a), film of PNDI2T2G-2Tz containing 40 mol% N-DMBI (b) and that containing 40 mol% PyDMBI (c), respectively. The red area indicates where dopants are present. The darker the red, the greater the distribution of dopants in that region. All the film were measured before annealing. The scare bar is 500 nm.

7. Theoretical calculation

To obtain a better description, the electronic-structure properties were calculated based on the optimized geometries by using the long-range corrected functional ωB97X with the range separation parameter ω optimally determined according to the gap-tuning procedure.[S2]

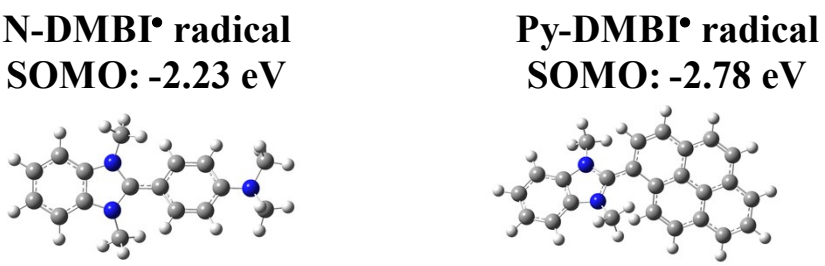

Fig. S12 Atomic-scale representation and the SOMO energy levels of the radicals of N-DMBI• and Py-DMBI•.

To generate molecular packing morphologies of the doped blend films, molecular dynamics (MD) simulations were performed by the Gromacs-4.6.7 package[S3] based on the general AMBER force field (GAFF)[S4] with the RESP charge[S5]. The torsion potential of highlight dihedral angle for the PNDI2TEG-2Tz were re-parametrized according to density functional theory (DFT) calculations at the B3LYP/6-311G** level (Fig. S13), as described in the previous work. [S6]The simulations were carried out under the NPT ensemble with three-dimensional periodic boundary condition using the leap-frog integrator with a time step of 1.0 fs. A cut-off of 1.2 nm for the summation of van der Waals interaction and short-range electrostatic interactions and the particle-mesh Ewald solver for long-range electrostatic interactions were used throughout. The velocity rescaling thermostat[S7] and the Berendsen barostat[S8] were applied to control the temperature and pressure, except for the final 50 ns of equilibration; the Nose-Hoover thermostat[S9, S10] and the Parrinello-Rahman barostat[S11] were used to obtain better equilibrium configurations.

The films of the doped PNDI2TEG-2Tz were simulated by the following procedure. We first constructed a 30 × 30 × 30 nm^3 box containing 20 PNDI2TEG-2Tz chains (each consists of 10 repeat units)，40 N-DMBI or Py-DMBI molecules, and 50000 chloroform molecules, being consistent with the experimental doping concentration of Py-DMBI or N-DMBI (20 mol% *vs.* the repeat unit of PNDI2TEG-2Tz). To make the polymer semiconductor, dopant, and solvent molecules disperse homogeneously and the system relaxed, we ran a 1 ns equilibration under high pressure (100 bar) and then a 20 ns equilibrated under normal pressure (1 bar). The solvent evaporation process was modelled by using a quasi-equilibrium approach, in which 100 chloroform molecules were randomly removed every 100 ps from the solution under 1 bar. After evaporation of solvent, the dried

film was further equilibrated for 50 ns under 1 bar. All the MD simulations were performed at 300 K. The last 10 ns of equilibration was sampled every 10 ps to produce 1000 snapshots to investigate the local morphology.

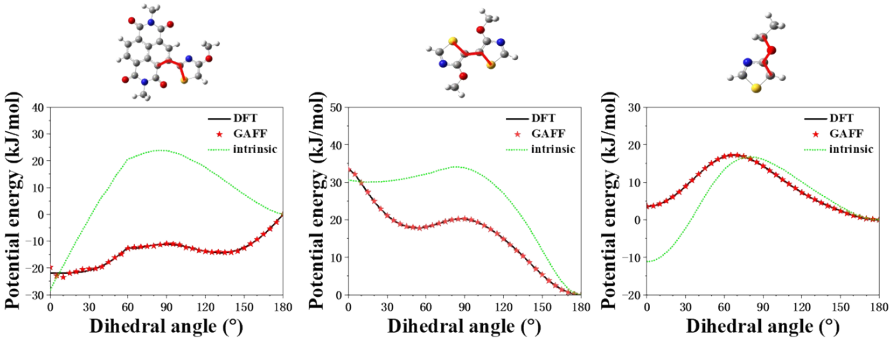

Fig. S13 Potential energies for the highlighted dihedral angles calculated by DFT and GAFF along with the fitted intrinsic torsion potentials of PNDI2TEG-2Tz.

8. Copies of NMR spectra

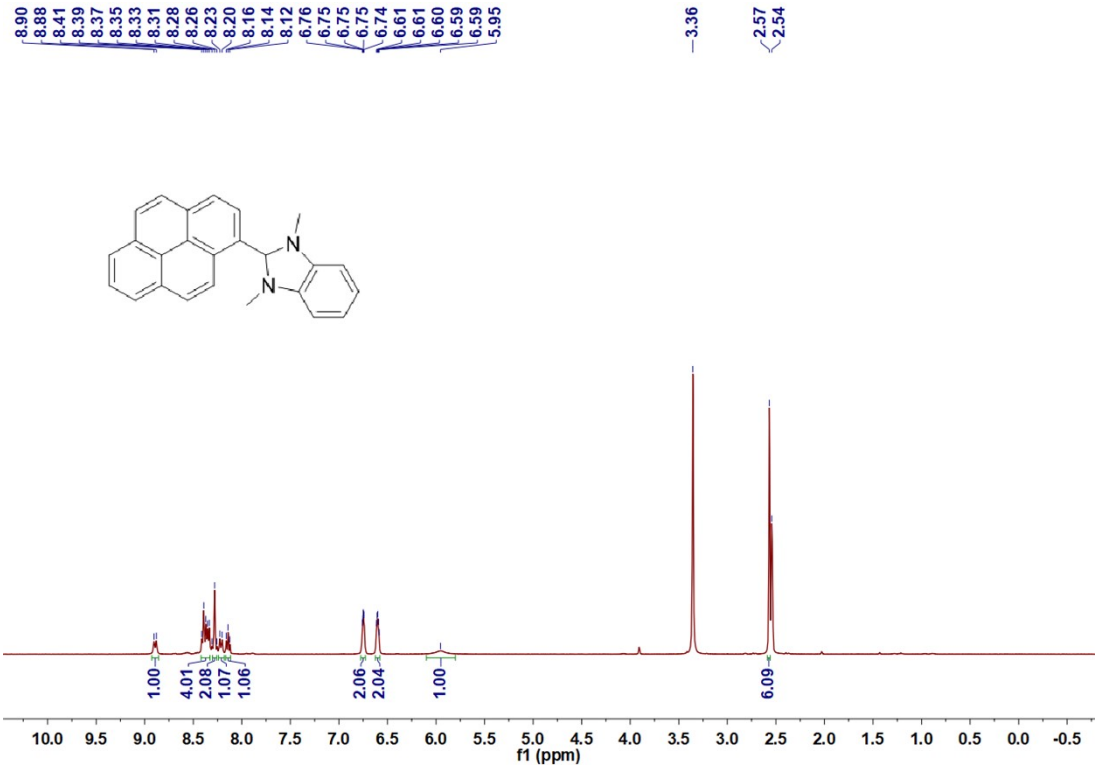

Fig. S14 ^{1}H NMR spectrum of Py-DMBI in DMSO-*d*6

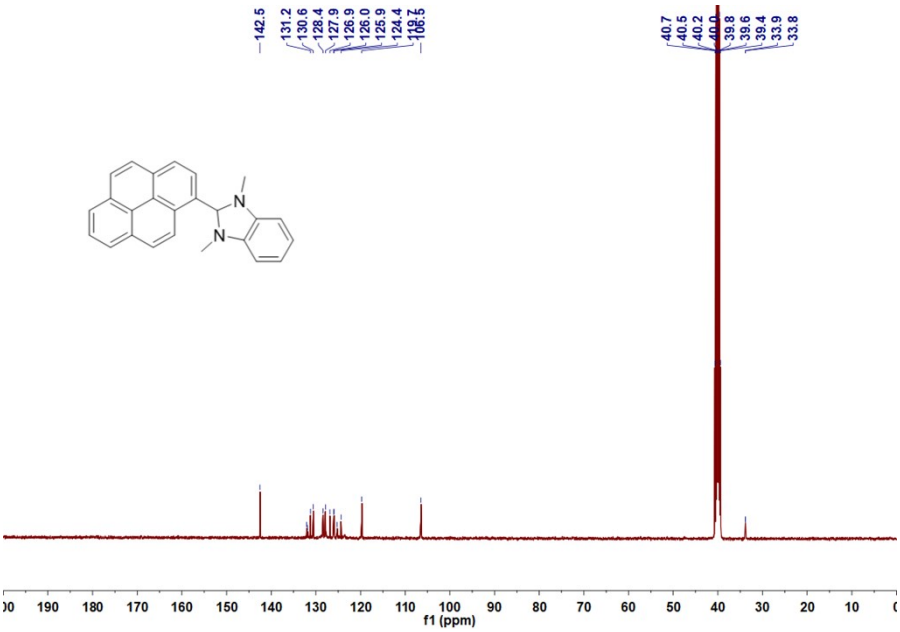

Fig. S15 ^{13}C NMR spectrum of Py-DMBI in DMSO-*d*6

9. Reference

[S1] Yan, X.; Xiong, M.; Li, J.; Zhang, S.; Ahmad, Z.; Lu, Y.; Wang, Z.-Y.; Yao, Z.-F.; Wang, J.-Y.; Gu, X.; Lei, T. *J. Am. Chem. Soc.*, 2019, **141**, 20215-20221.

[S2] Zheng, Z.; Brédas, J.-L.; Coropceanu, V., *J. Phys. Chem. Lett.* 2016, **7,** 2616-2621.

[S3] Hess, B.; Kutzner, C.; van der Spoel, D.; Lindahl, E., *J. Chem. Theory Comput.* 2008, **4**, 435-447.

[S4] Wang, J.; Wolf Romain, M.; Caldwell James, W.; Kollman Peter, A.; Case David, A., *J. Comput. Chem.* 2004, **25**, 1157-1174.

[S5] Bayly, C. I.; Cieplak, P.; Cornell, W.; Kollman, P. A., *J. Phys. Chem.* 1993, **97**, 10269-10280.

[S6] Han, G.; Guo, Y.; Song, X.; Wang, Y.; Yi, Y., *J. Mater. Chem. C* 2017, **5**, 4852-4857.

[S7] Bussi, G.; Donadio, D.; Parrinello, M., *J. Chem. Phys.* 2007**, 126**, 014101.

[S8] Berendsen, H. J. C.; Postma, J. P. M.; van Gunsteren, W. F.; DiNola, A.; Haak, J. R., *J. Chem. Phys.* 1984, **81**, 3684-3690.

[S9] Evans, D. J.; Holian, B. L., *J. Chem. Phys.* 1985, **83**, 4069-4074.

[S10] Nosé, S., *J. Chem. Phys.* 1984, **81**, 511-519.

[S11] Parrinello, M.; Rahman, A., *J. Appl. Phys.* 1981, **52**, 7182-7190.